A Lung Nodule Segmentation Using Python

Dr. Sivaranjani B[1], Ms. Swetha S[2], Ms. Ramya P[3], Mr. Srinivasan M[4]
[1]*II M. Sc Computer Science, Dr. N.G.P. Arts and Science College, Coimbatore-48, Tamil Nadu, India*
[2]*M.Sc., M.Phil., Ph.D., Assistant Professor, Department of Computer Science, Dr. N.G.P. Arts and Science College, Coimbatore-48, Tamil Nadu, India*

***Abstract*—Lung nodule segmentation in CT images plays an important role in clinical diagnosis and treatment of lung cancers. Among different types of nodules, the solitary nodules usually have clear boundaries and the segmentation is relatively easy, while the segmentation of non-solitary nodules with ambiguous boundaries remains challenging for both human and computer. In this paper, we propose a coarse-to-fine lung nodule segmentation method by combining image enhancement and a Dual-branch neural network. First, we preprocess the image to enhance the discrimination of the nodules and roughly locate the lesion area so that we can eliminate the noises from background and focus on learning the features around the boundaries. Second, we propose a Dual-branch network based on U-Net (DB U-Net) which can effectively explore information from both 2D slices and the relationships between neighboring slices for more precise and consistent segmentation. In addition, we construct a dataset which is mainly composed of non-solitary nodules. The proposed image enhancement method improves the effectiveness of network learning, while the dual-branch neural network explores multi-view information. The Dice coefficients of nodule segmentation on the LIDC dataset and our own dataset are 83.16% and 81.97% respectively, which significantly outperforms the existing works.**

***Index Terms*—CT image, Dual-branch network, Image enhancement, Lung nodule segmentation, Non-solitary nodule**

I. INTRODUCTION

The task of lung nodule segmentation in CT (Computed Tomography) images is to label the boundariesof nodules, which is of great importance in the quantitative analysis and diagnosis of lung nodules [1]. For instance, VDT (Volume Doubling Time) and MDT (Mass Doubling Time) can be measured based on nodule segmentation, which play a guiding role in the diagnosis and treatment of lung nodules. In medical practice, nodules less than 10mm in diameter are usually monitored by continuous CT examinations to determine whether they are malignant tumors. The doubling time of a malignant tumor is generally 30 to 500 days, with an average of 100 days [2]. This time of 500 days is generally accepted as the upper limit of the doubling time for malignant pulmonary lesions [3]. Nodules enlarged in a short term (VDT<20) or stable for a long term (VDT>500) are more likely to be benign ones. The small benign nodules are mainlycontrolled by drugs. Nodules with VDT between 30 and 500 are likely to be malignant tumors and need further surgical treatment. The calculations of VDT and MDT need precise and consistent segmentation of nodules. Manual segmentation is usually impractical. First, a CT image consists of tens to hundreds of slices. Labelling the boundaries is thus labor-expensive. Second, since the bound- ary of the nodule is usually ambiguous, the labelling is sometimes objective and the segmentation results by different people at different time are usually inconsistent. In this case, the quantitative analysis would be imprecise. For instance, the calculation of MDT and VDT need to do the nodule segmentation two or more times, and the consistency of segmentation result is crucial. To address these problems, it is necessary to develop automatic or computer-aided lung nodule segmentation methods.

In the past few decades, many approaches for segmentation [13]. Marcin et al. uses local variance and probabilistic neural networks to complete the detection of lung nodules, and achieves a high accuracy [14]. Cao et al. propose a Dual-branch Residual Network (DB- ResNet) to segment lung nodules, which can effectively cap- ture multi-view and multi-scale features of different nodules in CT images [15]. Ilaria used a 3d convolutional neural network to assess nodule malignancy and integrated it in an automated end-to-end existing pipeline of lung cancer detec- tion

[16]. Wang et al. propose a mixed-supervised dual network for medical image segmentation. The model uses two independent networks to perform detection and segmentation tasks, which works well for the lung nodule segmentation task [17].Junhua Gu proposes an improved detection model of lung nodules based on deformation convolution, which
combined with a simple and effective lung nodule size vvariation strategy so that the model can effectively fuse the feature maps of different sizes [18]. Tang et al. propose a new end-to-end 3D deep convolutional neural network, and good results are obtained in both lung nodule detection and segmentation tasks [19]. Xin Z. et al. propose an improved pyramid deconvolution neural network that can effectively segment lung nodules [20]. In addition, some other networks such as U-Net and R-CNN originally developed for common image segmentation are also used in the segmentation of lung nodules [27]–[29].
Since the consecutive slices of CT images are closely related, the use of multiple slices in CT images to enhance the performances of deep learning models has also been studied and explored. Lei et al. propose a new classification method of lung nodules, which uses multiple CT slices as input to alleviate the model overfitting problem, and thereby improve the prediction performance [32].
Fig. 1 illustrates some examples of different types of lung nodules. Among them, the boundary of solitary nodule is usually clear, and the segmentation is relatively easy. For the other nodules, the boundaries are ambiguous and the segmentation can be greatly affected by background noises. Most samples in public datasets are solitary nodules and the existing approaches work well for this kind of nodules. However, due to the sparsity of non-solitary nodules in the dataset, the model cannot be well trained to cope with these hard cases. The segmentation of non-solitary nodules remains challenging and has not been seriously studied. In this paper, we focus on the segmentation of non-solitary nodules. To this end, we propose a novel coarse-to-fine approach by integrating image enhancement and deep learning approaches. Given a CT image, image enhancement is first used to improve the discrimination of nodules and roughly locate the lesion area. Then, we propose a dual-branch segmentation network to label the precise boundaries of nodules, and combined ad- jacent slices of CT images in the network. Image processing approach requires less training data, while the deep learning approach is more robust. With this two-stage approach, we reduce the noise from non-lesion area so that the network can focus on learning the features around the boundaries. Both the efficiency and the effectiveness of learning are improved. Our experiments show that the proposed method significantly outperforms existing works especially for non-solitary lung nodule segmentation.

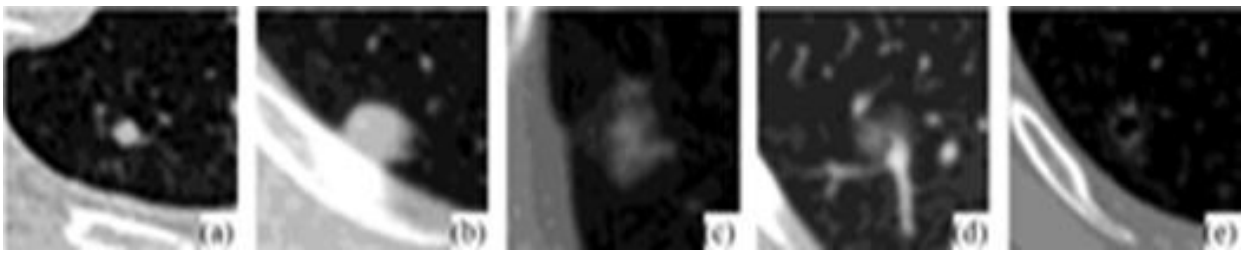

FIGURE 1: Different types of lunge nodules : (A)Solitary Nodule, (B)Juxta-Pleural Nodule, (C) Ground-Glass Nodule, (D)Juxta-Vascular Nodule, (E) Hollow Nodule

II. METHOD

Our method mainly consists of two stages. First, we locate the lesion based on image enhancement (LLIE). Second, inside the lesion area, we employ a dual-branch network based on U-Net (DB U-Net) to label the precise boundaries of lung nodules.

A. LESION LOCALIZATION BASED ON IMAGE ENHANCEMENT

We focus on labelling the boundaries of nodules while nodule detection is beyond the scope of this paper. The inputs are the CT images and the locations of the lung nodules (one point around the center of each nodule selected by human or nodule detection algorithms). Our method consists of four steps:
1) CT image conversion 2) contrast enhancement, 3) lung parenchyma separation, 4) lesion localization with region growing.

1) CT image conversion

Before image enhancement, we apply an intensity transfor- mation in the CT image to convert the CT value of each pixel to a grayscale value from 0 to 255. Except for bone tissue, the CT values of lung CT images are mostly distributed between -1000 HU to 400 HU, and a linear transform is employed.

$$\tilde{I}(x,y) = \begin{cases} 0, & I(x,y) < -1000 \\ \frac{I(x,y)+1000}{1600} * 255, & -1000 <= I(x,y) <= 400 \\ 255, & I(x,y) > 400 \end{cases}$$

where $I(x, y)$ and $\tilde{I}(x, y)$ are the original CT value and the transformed grayscale value respectively.

2) Contrast enhancement

Contrast enhancement aims at enhancing the contrast be- tween the nodules and the background so that the nodules are more discriminative for human and computer. This is impor- tant especially for non-solitary nodules where the boundaries are usually ambiguous as shown in Fig. 1. Here we employ histogram equalization algorithm as follows:

1) Count the number of pixels n_i in each gray level i, $i \in [0, 255]$.
2) Calculate the occurrence probability of each gray value in the image, $p_i = {}^{n_i}$, where n is the total number of

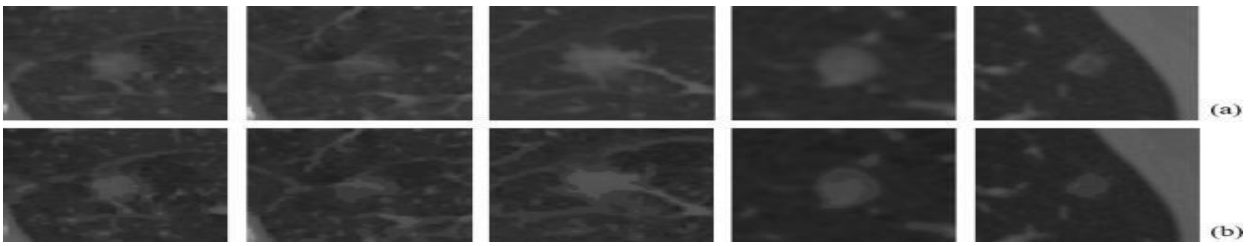

FIGURE 2. Some examples of image enhancement. (a) Original images, (b)Results after contrast enhancement

FIGURE 3. Lung parenchyma segmentation. (a) Original image, (b) The result after global-threshold binarization, (c) The result of morphology opening operation, (d) The result after removing the lung walls, (e) The patch cut around the lesion.

3) Lung parenchyma segmentation

We employ the global-threshold binarization to segment lung parenchyma from images. In this way, we can eliminate the noises from the walls of lung parenchyma as illustrated in Fig. 1(b) in nodule segmentation. The global-threshold binarization method works as follows.

1) Initially set the global threshold T = (Pmax + Pmin)/2, where Pmax and Pmin are the maximum and minimum pixel values of in the image.
2) Use T as the threshold to divide the image into fore- ground (gray value greater than or equal to T) and background (gray value less than T). Calculate the average gray value TF of the foreground and the average gray value TB of the background.
3) Update threshold T = (TF + TB)/2.
4) Repeat steps ii and iii until T no longer changes.

Fig. 3(b) shows the result of the binarization of the given CT image. After image binarization, we use morphological opening operation to remove the noises of lung walls, and the result is shown in Fig. 3(c). Fig. 3(d) shows the segmented lung parenchyma. Finally, we cut a patch with the size of W × H centering at the input point as shown in Fig.

3(e). In our experiment, we set W = H = 64 so that the whole nodules can be included.
pixels in the image. n

3) Accumulate p_i to get $cdf_i = \sum_{j=0}^{i} p_i$.
4) Implement grayscale conversion: $H_i = cdf_i * 255$ where i is the original gray value, and H_i is the converted gray value.

Fig. 2 shows some examples of contrast enhancement. By histogram equalization, the contrast between nodules and backgrounds are enhanced.

We use the region growing method to roughly locate the lesion area, which works as follows.

1) Set the center of the image as the seed point (x0, y0) as shown in Fig. 4(a).
2) Taking the point (x0, y0) as the center, consider the 8 neighborhood pixels (x, y) of P in turn. If P (x0, y0) and P (x, y) are the pixel values of (x0, y0) and (x, y) respectively, then merge (x, y) and (x0, y0) into one region.
3) Use the newly merged points as the new seed points, and repeat step ii until all eligible points around the nodule are visited.

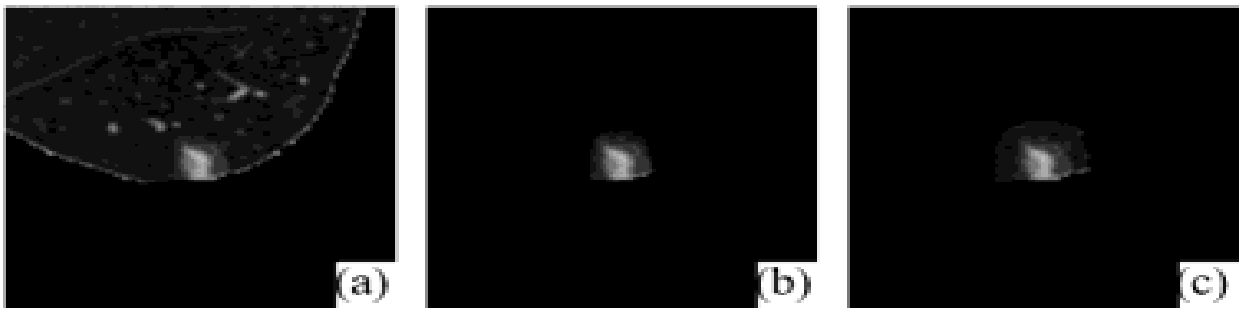

FIGURE 4. Nodule region growing. (a) Seed point, (b) The result after region growing, (c) The result of morphology dilatation operation.

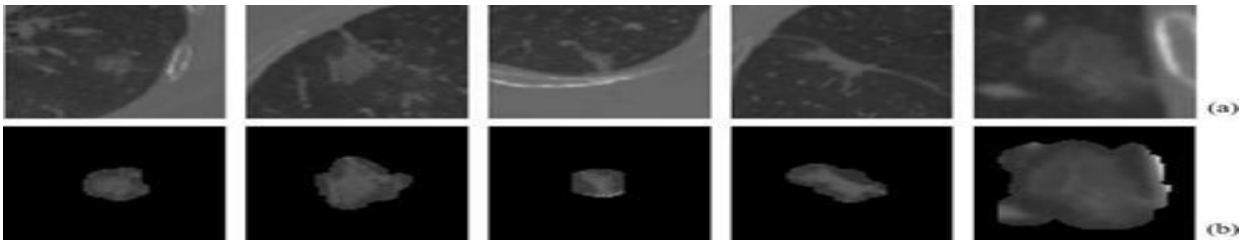

FIGURE 5. Some examples of lesion localization with image enhancement.
(a) Original images, (b) The results of lesion localization.

In our implementation, we empirically set T = 3 which can effectively include the lung nodules without too much background. Fig. 4(b) shows an example of lung nodule region growing. To ensure that the lung nodules are included in the area after the region growing, we further perform morphological dilation operation as shown in Fig. 4(c). Fig. 5 shows some examples after the nodule localization with LLIE operation. Compared with the original images, after LLIE, the lung nodule is located in a smaller area, which helps fine segmentation by removing irrelevant noises and improving the discrimination between the nodules and the background. Furthermore, by lesion localization, the neural network can focus on learning the features around the boundaries of the nodules, which can improve the efficiency and the effective- ness of network training with less images.

B. DUAL-BRANCH NETWORK FOR NODULE SEGMENTATION

After roughly locating the lung nodules, we propose a dual- branch network based on U-Net (DB U-Net) for fine segmen- tation. Our network consists of a 2D U-Net branch to capture the information from 2D CT slices and a 3D U-Net branch to capture the relationships between neighboring slices.

1) 2D U-Net and 3D U-Net

2D U-Net proposed in [21] is widely used in image seg- mentation. As shown in Fig. 6(b), the U-Net network is composed of two parts. The first part is used for feature extraction, and the second part for up-sampling. 3D U-Net proposed in [22] is derived from 2D U-Net by replacing the 2D convolution with 3D convolution. At the same time, in

order to speed up convergence and avoid training bottlenecks, Batch Normalization (BN) is used.

Each CT image is composed of a number of slices. When using 2D U-Net to segment a 3D object, the input slices are processed independently. However, the consecutive slices in a CT image are closely related to each other. Compared with 2D U-Net, 3D U-Net network can effectively explore the relationships between neighboring slices to produce more consistent and accurate boundaries for the nodules.

On the other hand, the complexity of 3D network is usually much higher, and it is impossible to take the entire image as input. The original image need to be cropped. However, cropping will limit the maximum receptive field that the network can reach, which will result in the loss of certain global information. Thus, 3D U-Net can only focus on the local features.

In summary, 2D U-Net has lower hardware requirements, but cannot capture spatial relationships between neighboring slices. 3D U-Net can effectively capture multi-view infor- mation, but has higher hardware requirements. Thus, in this paper, we combine these two types of networks by proposing a dual-branch network based on U-Net. The unique dual- branch structure allows it to effectively combine the features from multiple views.

2) Dual-branch network based on U-Net

Our proposed network is composed of two deep branches that share the same structure, while the inputs are different. As shown in Fig. 6, the two branches use 2D and 3D CT images for lung nodule segmentation respectively. For a given CT image, different from 2D branch input, the 3D branch uses a 3-layer CT image (3 images taken from the previous, the current, and the next slices) as inputs. The significance of the dual-branch structure is to capture multi-view features from multiple slices of CT images.

As shown in Fig. 6, the network includes a dual-branch structure and a 1×1 convolution layer. The dual-branch struc- ture adopts the model based on U-Net. The model includes four encoders and four decoders. Each encoder includes the repeated operations of two 3 × 3 convolutions and one

2 × 2 maximum pooling with stride 2 for down-sampling. At each down-sampling step, we double the number of feature channels. The decoder uses the output of the corresponding encoder and the up-sampling result of the previous step as input. After two 3 × 3 convolutions, an up-sampling oper- ation is performed. After each convolution, there is a batch normalization operation and a rectified linear unit (ReLU). Each branch includes 22 convolutional layers. At the end of the model, the features generated by the two branches are concatenated, and the result of concatenation is fed to a 1 × 1 convolution layer which generates the final segmentation result.

III. RESULTS

C. DATASETS AND SETTINGS

The following two datasets are used in our experiments.

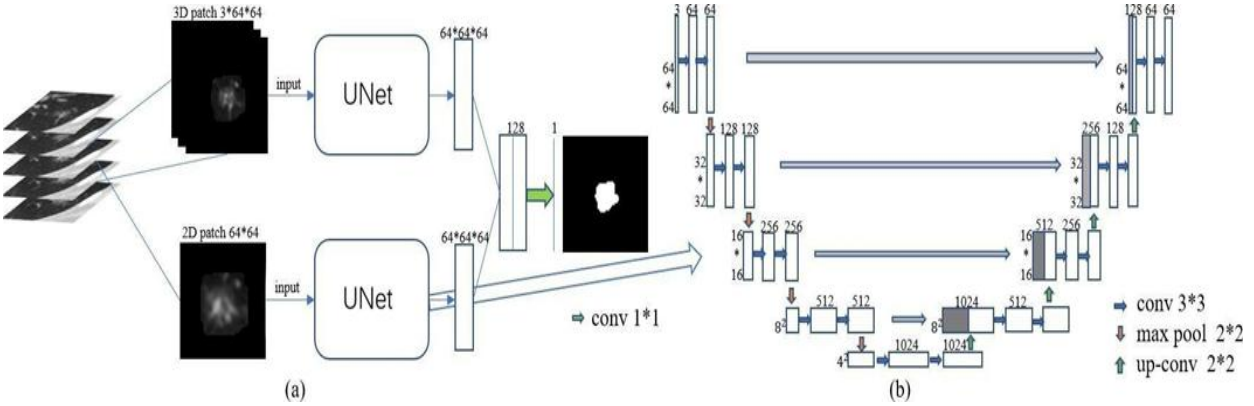

FIGURE 6. (a) The structure of DB U-Net; (b) The detailed structure of U-Net in (a).

• LIDC dataset: This is a publicly available dataset of the Lung Image Database Consortium and Image Database Resource Initiative. We select 964 samples consisting of 6,388 CT images of lung nodules. Most nodules in this dataset are solitary. All samples were labeled by four radiologists. In this dataset, we randomly divide all samples into three subsets for training (624 samples), validation (50 samples), and testing (290 samples). The three subsets have similar statistical distributions. We train the neural network model on the training set, and the validation set is used to determine the number of training epochs. Finally, the test set is used for perfor- mance evaluation.

• SHCH dataset: The second dataset is collected from Shanghai Chest Hospital and consists of 82 patients with lung nodules. Most nodules are small (less than 6mm in diameter) and non-solitary. To evaluate the segmentation results, we use dice similarity coefficient (DSC) as the primary criterion. DSC is widely used to measure the degree of overlap between two segmen- tation results. To ensure the robustness of the evaluation, we also use the positive prediction value (PPV) and sensitivity (SEN) as auxiliary evaluation metrics. These metrics are calculated as: 2 ∗ V (G ∩ S) initial learning rate to 0.0001. The model is accelerated on an NVIDIA TITAN Xp GPU.

TABLE 1. Segmentation result on LIDC dataset, the best performance is indicated in bold font.

Method	DSC(%)	SEN(%)	PPV(%)
2D U-Net [21]	80.11 ± 11.34	86.04 ± 16.43	79.30 ± 13.08
2D U-Net + LLIE	81.27 ± 11.76	87.83 ± 15.41	79.14 ± 14.57
3D U-Net [22]	81.15 ± 10.69	87.61 ± 14.40	78.18 ± 15.13
3D U-Net + LLIE	82.06 ± 11.46	87.78 ± 13.57	78.65 ± 14.72
DB U-Net	82.98 ± 10.19	88.17 ± 12.07	79.66 ± 13.30
DB U-Net + LLIE	83.16 ± 11.28	88.51 ± 12.13	78.98 ± 14.62

The training of deep neural networks generally requires a large number of samples. However, the cost of collecting medical images is quite high and thus most medical image datasets are relatively small. To cope with the lack of training samples, we implement a series of data augmentation opera- tions including horizontal/vertical flipping of images, random rotation, random cropping, and deformation. Through these operations, the number of training samples is increased by 5 times, and the data distribution is more diversified so that the model has better generalization capabilities. These operations are carried out in real-time during training.

C. RESULTS ON LIDC DATASET

Table 1 presents the performance of our proposed method on the LIDC dataset. As can be observed in Table 1, the proposed DB U-Net model outperforms 2D U-Net and 3D U-Net. This shows that DB U-Net can effectively explore the spatial relationship between neighboring slices for accurate segmentation.After further employing the LLIE strategy, the perfor- mances of different models are improved.where G is the lesion region in the groundtruth, S is the segmentation result, and V (.) is the volume size calculated in voxel units.

$$DSC = \frac{2 * V(G \cap S)}{V(G) + V(S)}$$

$$SEN = \frac{V(G \cap S)}{V(G)}$$

$$PPV = \frac{V(G \cap S)}{V(S)}$$

where G is the lesion region in the groundtruth, S is the segmentation result, and V (.) is the volume size calculated in voxel units.

D. IMPLEMENTATION DETAILS

We employ Pytorch in our implementation. The Dice loss is

TABLE 2. The results for various segmentation methods

Method	DSC(%)	SEN(%)	PPV(%)
FCN [31]	79.11 ± 11.21	84.52 ± 13.27	78.25 ± 12.69
Deeplab V1 [24]	78.87 ± 12.01	83.38 ± 14.22	78.04 ± 14.41
MV-CNN [30]	78.61 ± 12.54	84.57 ± 11.79	76.97 ± 14.73
CF-CNN [12]	81.18 ± 11.91	89.75 ± 12.23	76.46 ± 13.51
Our method	83.16± 11.28	88.51 ± 12.13	78.98± 14.62

TABLE 3. Segmentation results with our method on SHCH dataset. The difference in the training set represents the two experiment settings

Method	Training set	DSC(%)
DB U-Net	LIDC	78.01 ± 12.23
DB U-Net	SHCH	80.56 ± 10.79

D. RESULTS ON SHCH DATASET

We use the SHCH dataset to further verify our proposed method. Compared with LIDC dataset where most nodules are solitary, the nodules in SHCH dataset are mainly non- solitary. For model training, we experiment two different settings: i) We use LIDC dataset as training set and SHCH dataset as testing set to evaluate the segmentation perfor- mance of the model; ii) We divide SHCH dataset into training set and testing set for evaluation.

Table 3 presents the experimental results with these two different settings. As can be seen in Table 3, by re-training the models with SHCH dataset, the DSC is improved by 2.55%. Since most samples in LIDC dataset are solitary nodules, the model cannot be well trained to cope with the non-solitary nodule segmentation in SHCH dataset due to the special mist structures. Instead, the SHCH dataset can be used for model training with non-solitary nodules.

Table 4 presents the performances of different models on SHCH dataset. Compared with single-branch networks such as 2D U-Net and 3D U-Net, the dual-branch model performs significantly better since the dual-branch network can effectively combine the multi-view features of the CT images. By employing LLIE to preprocess the images and locate the lesion, the DSC is improved by 1.41%. This shows that our proposed LLIE method can effectively cope with the ambiguous boundaries of non-solitary nodules during segmentation.

Table 5 presents the efficiency of model training with and without LLIE. After using the LLIE strategy, the training of the model is significantly faster. By first locating the lesion area, the model can focus only on smaller regions and ignore most background information. On one hand, this speeds up
the training process; on the other hand, the noises from irrelevant regions are eliminated and thus the segmentation accuracy is improved.

TABLE 4. The results for various segmentation methods

Method	DSC(%)	SEN(%)	PPV(%)
2D U-Net [21]	78.95 ± 11.19	79.24 ± 13.18	78.82 ± 13.62
2D U-Net+LLIE	80.28 ± 10.79	81.30 ± 14.90	79.95 ± 14.13
3D U-Net [22]	78.75 ± 11.31	81.42 ± 15.23	77.66 ± 13.68
3D U-Net+LLIE	80.71 ± 11.21	83.23 ± 14.19	79.27 ± 12.38
DB U-Net	80.56 ± 10.79	82.74 ± 13.94	78.26 ± 11.71
DB U-Net+LLIE	81.97 ± 10.16	84.57 ± 14.79	79.33 ± 14.08

TABLE 5. The efficiency of model training

Method	DSC(%)	Epoch	Training time (hours)
DB U-Net	80.56 ± 10.79	150	2.24
LLIE+DB U-Net	81.97 ± 10.16	50	0.98

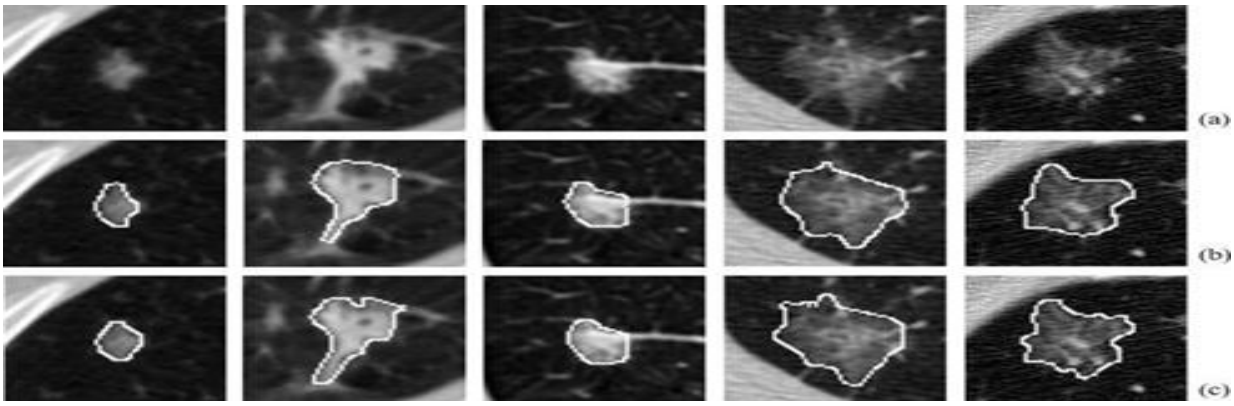

FIGURE 7. Some examples of lung nodule segmentation results. (a) Original images, (b) Segmentation results of our method, (c) Segmentation results of groundtruth.

IV. DISCUSSION

Accurate and consistent segmentation of lung nodules is important for the diagnosis and treatment of lung cancers. Compared with human, computer is better at promising the consistency of segmentation criterions and results for dif- ferent cases at any time. This characteristic is crucial for some quantitative analysis such as the calculation of VDT and MDT during the diagnosis. Among different types of nodules, the boundaries of solitary nodules are basically clear and the segmentation is relatively easy. However, the boundaries of non-solitary nodules are usually ambiguous which bring much difficulty to both human and automatic segmentation. Most existing public datasets are mainly com- posed of solitary nodules and do not pay extra attentions to non-solitary nodules. Thus, the models cannot be well trained to cope with the ambiguous boundaries of non-solitary nod- ules. In this work, we construct a dataset which contains mainly non-solitary nodules. Our experiments show that re- training the model on the new dataset (although small) can significantly improve the segmentation results.

Our DB U-Net+LLIE model achieves an accuracy of 81.97% on our new dataset of non-solitary nodules. Over- all, the performance is quite satisfactory according to the expert radiologists' feedbacks. Fig. 7 shows some examples of our method compared with the groundtruth labels. Most segmentation results of our method are well alighed with the groundtruth.

However, few lung nodules are poorly segmented as shown in Fig. 8, which are mainly hollow nodules and thin film- like ground-glass nodules. According to our analysis, hollow nodules are difficult to identify due to the existence of holes in the interior and lack of training data. Some ground-glass nodules are difficult to segment since their pixel values are very close to the background. For future work, to cope with these special cases, we can adopt the divide-and-conquer strategy by first classifying the nodules and then employing different methods according to the types of the nodules.

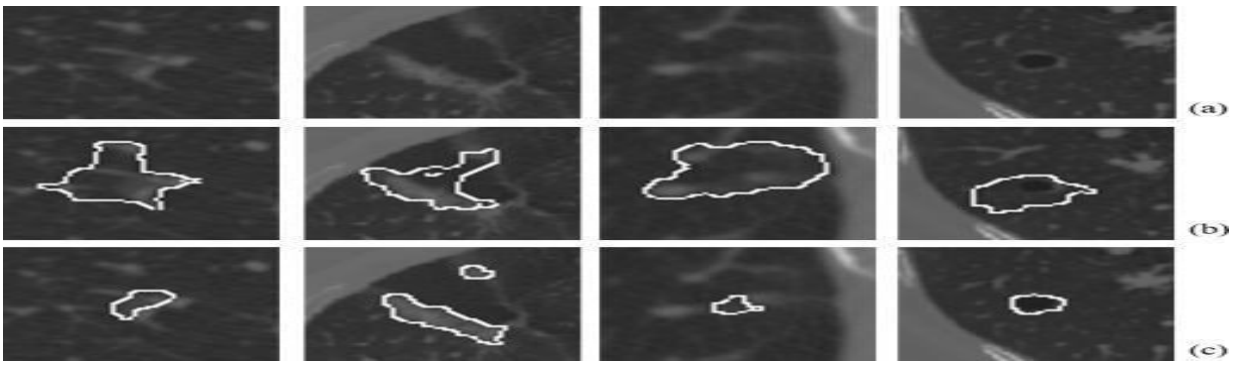

FIGURE 8. Examples of poor segmentation. (a) Original images, (b) Segmentation results of our method, (c) Segmentation results of groundtruth.

V. CONCLUSIONS

In this article, we have presented our lung nodule segmen- tation method which combines image enhancement and a Dual-branch network based on U-Net (DB U-Net). By first roughly locating the lesion based on image enhancement, we improve the discrimination of nodules and eliminate the noise from non-lesion area, which can improve the efficiency and the effectiveness of network learning. The two branches of DB U-Net integrates the information in each slice and the spatial relationship between neighboring slices for more accurate and consistent segmentation. Our experiments show that the proposed method significantly outperforms the state- of-the-art methods, especially for the non-solitary nodule segmentation. The performance could be further improved by training the model with more images. In future work, we will attempt dual-branch networks with different structures, and integrate expert knowledge into neural networks for potential improvement.

REFERENCES

[1] C. Xu, K. Hao, Y. Song, L. Yu, Z Hou, and P. Zhan. "Early diagnosis of solitary pulmonary nodules". Journal of Thoracic Disease., vol. 5(6), pp. 830–840, Dec. 2013.

[2] M. P. Revel, A. Merlin, S. Peyrard, R. Triki, S. Couchon, G. Chatellier, and G. Ferja. "Software volumetric evaluation of doubling times for differentiating benign versus malignant pulmonary nodules". American Journal of Rentgenology., vol. 187(1), pp. 135–142, Jul. 2012.

[3] H. T. WinerMuram, S. G. Jennings, R. D. Tarver, A. M. Aisen, M. Tann, J. Conces, and C. A. Meyer "Volumetric growth rate of stage I lung cancer prior to treatment: serial CT scanning". Radiology., vol. 223(3), pp. 798–805, Jun. 2002.

[4] X. Ye, X. Lin, J. Dehmeshki, G. Slabaugh, and G Beddoe. "Shape-Based Computer-Aided Detection of Lung Nodules in Thoracic CT Images". IEEE Transactions on Biomedical Engineering., vol. 56(7), pp. 1810– 1820, Jun. 2009.

[5] J. Dehmeshki, H. Amin, M. Valdivieso, and X. Ye. "Segmentation of Pulmonary Nodules in Thoracic CT Scans: A Region Growing Approach". IEEE Transactions on Medical Imaging., vol. 27(4), pp. 467–480, Mar. 2008.

[6] W.J. Kostis, A.P. Reeves, D.F. Yankelevitz, and C.I. Henschke. "Three- dimensional segmentation and growth-rate estimation of small pulmonary nodules in helical CT images". IEEE Transactions on Medical Imaging., vol. 22(10), pp. 1259–1274, Sep. 2003.

[7] N. Chen, G. Liu, Y. Liao, C. Ou, and Y. Yu. "Research on computer-aided diagnosis of lung nodule". IEEE Workshop on Electronics, Computer and Applications., pp. 8–9, May. 2014.

[8] V. V. Kishore, and R. V. S. Satyanarayana. "Performance evaluation of edge detectors - morphology based ROI segmentation and nodule detection from DICOM lung images in the noisy environment". IEEE International Advanced Computing Conference., pp. 22–23, Feb. 2013.

[9] J. Muzzamil, J. Moazzam, M. Z. U. Rehmana, and S. I. A. Shah. "A novel approach to CAD system for the detection of lung nodules in CT images". Computer Methods and Programs in Biomedicine., vol. 135, pp. 125–139, Oct. 2016.

[10] J. M. Kuhnigk, V. Dicken, L. Bornemann, A. Bakai, D. Wormanns, S. Krass, and H. O. Peitgen. "Morphological segmentation and partial volume analysis for volumetry of solid pulmonary lesions in thoracic CT scan". IEEE Transactions on Medical Imaging., vol. 25(4), pp. 417–434, Mar. 2006.

[11] T. Kubota, A. K. Jerebko, M. Dewan, M. Salganicoff, and A. Krishnan. "Segmentation of pulmonary nodules of various densities with morpho- logical approaches and convexity models". Medical Image Analysis., vol. 15(1), pp. 133–154, Feb. 2011.

[12] S. Wang, M. Zhou, Z. Liu, Z. Liu, D. Gu, Y. Zang, D. Dong, O. Gevaert, and J. Tian. "Central focused convolutional neural networks: Developing a data-driven model for lung nodule segmentation". Medical Image Anal- ysis., vol. 40, pp. 172–183, Aug. 2017.

[13] X. Huang, W. Sun, T. L. Tseng, C. Li, and W. Qian. "Fast and fully- automated detection and segmentation of pulmonary nodules in thoracic CT scans using deep convolutional neural networks". Computerized Med- ical Imaging and Graphics., vol. 74, pp. 25–36, Jun. 2019.

[14] W. Marcin, P. Dawid, G. Capizzi, G. L. Sciuto, L. Kosmider, and K. Frankiewicz. “Small lung nodules detection based on local variance analysis and probabilistic neural network”. Computer Methods and Programs in Biomedicine., vol. 161, pp. 173–180, Jul. 2018.

[15] H. Cao, H. Liu, E. Song, C. C. Hung, G. Ma, X. Xu, R. Jin and J. Lu. “Dual-branch residual network for lung nodule segmentation”. Applied Soft Computing Journal., vol. 86, 105934, Jan. 2020.

[16] I. Bonavita, X. R. Palou, M. Ceresa, G. Piella, V. Ribas, and M. A. G. Ballester. “Integration of convolutional neural networks for pulmonary nodule malignancy assessment in a lung cancer classification pipeline”. Computer Methods and Programs in Biomedicine., vol. 185, 105172, Mar. 2020.

[17] D. Wang, M. Li, N. B. Shlomo, C. E. Corrales, Y. Cheng, T. Zhang, and J. Jayender. “Mixed-Supervised Dual-Network for Medical Image Segmen- tation”. Medical Image Computing and Computer Assisted Intervention., pp. 192–200, Oct. 2019.

[18] J. Gu, Z. Tian, and Y. Qi. “Pulmonary Nodules Detection Based on Deformable Convolution”. IEEE Access., vol. 8, pp. 16302–16309, Jan. 2020.

[19] H. Tang, C. Zhang, and X. Xie. “NoduleNet: Decoupled False Positive Reductionfor Pulmonary Nodule Detection and Segmentation”. Medical Image Computing and Computer Assisted Intervention., pp. 266–274, Oct. 2019.

[20] X. Zhao, W. Sun, W. Qian, S. Qi, J. Sun, B. Zhang, and Z. Yang. “Fine- grained lung nodule segmentation with pyramid deconvolutional neural network”. SPIE Medical Imaging., vol. 10950, pp. 6. Mar. 2019.